FISEVIER

Contents lists available at ScienceDirect

Journal of Luminescence

journal homepage: www.elsevier.com/locate/jlumin



The impact of ${}^2H_{9/2} \rightarrow {}^4I_{13/2}$ emission from Er^{3+} ions on ratiometric optical temperature sensing with Yb^{3+}/Er^{3+} co-doped upconversion materials

Xiaojing Xia^{a,*}, Azzurra Volpi^b, Joo Yeon D. Roh^c, Michael De Siena^{c, d}, Daniel R. Gamelin^c, Markus P. Hehlen^{d, 1}, Peter J. Pauzauskie^{e, f, **}

- ^a Molecular Engineering & Science Institute, University of Washington, Seattle, WA, 98195, USA
- b Physics & Astronomy and Interdisciplinary Science, University of New Mexico, Albuquerque, NM, 87131, USA
- ^c Department of Chemistry, University of Washington, Seattle, WA, 98195, USA
- ^d Space & Remote Sensing (ISR-2), Los Alamos National Laboratory, Los Alamos, NM, 87545, USA
- e Department of Materials Science & Engineering, University of Washington, Seattle, WA, 98195, USA
- f Fundamental & Computational Sciences Directorate, Pacific Northwest National Laboratory, Richland, WA, 99352, USA

ARTICLE INFO

Keywords: Temperature sensing Upconversion Fluorescent intensity ratio Yb³⁺/Er³⁺ co-doped

ABSTRACT

Yb $^{3+}$ /Er $^{3+}$ co-doped upconversion materials are widely used for luminescence intensity ratio (LIR) thermometry, where the relative intensity ratio of the green luminescence transitions ($^2H_{11/2} \rightarrow ^4I_{15/2}$ and $^4S_{3/2} \rightarrow ^4I_{15/2}$) of Er $^{3+}$ dopant ions changes with temperature. In this work we report on the impact of an additional transition from the $^2H_{9/2}$ level to the intermediate $^4I_{13/2}$ level, which overlaps with the green luminescence normally used for LIR thermometry. The $^2H_{9/2} \rightarrow ^4I_{13/2}$ emission overlaps extensively with the $^4S_{3/2} \rightarrow ^4I_{15/2}$ emission and is more sensitive to pump power. The wavelength intervals used to integrate both $^2H_{11/2} \rightarrow ^4I_{15/2}$ and $^4S_{3/2} \rightarrow ^4I_{15/2}$ luminescence need be selected carefully in order to achieve accurate temperature readouts.

1. Introduction

The precise and accurate measurement of temperature is crucial for many advanced technological applications including but not limited to microelectronics, bio-medicine, and aerospace [1]. Present technological demands in microelectronics and nanoelectronics, microfluidics, and nanophotonics, among others, have developed to the point that conventional contact thermal probes are no longer able to perform accurate measurements with sub-micron spatial resolution without detrimental electromagnetic interference. These increasing demands for accurate nanoscale thermometry have stimulated the development of novel non-contact thermal probes based on luminescence thermometry [2–6].

Luminescence thermometry based on trivalent lanthanide ions has increased in popularity over the last several years due to the unique versatility, stability, and narrow emission band profiles of the ions that cover the entire electromagnetic spectrum with relatively high emission quantum yields [1,7]. Changes on luminescence features such as inten-

sity, bandwidth, spectral shift, lifetime and polarization are possible effects caused by temperature variations. Among them, luminescence intensity ratio (LIR, sometimes referred as fluorescence intensity ratio, FIR, when transitions obey the spin selection rule) and luminescence lifetime are the two most promising luminescence-based temperature sensing techniques. In LIR thermometry, the change in the intensity ratio of two transitions is used to measure temperature [8]. The LIR (Δ) is defined in Eq. (1) using the emission intensities (photons per unit time) of the $|2>\rightarrow|0>$ and $|1>\rightarrow|0>$ transitions, where |0> denotes the ground level and |1> and |2> the two thermally coupled excited levels (level |2> is more energetic than level |1>)

$$\Delta = \frac{I_2}{I_1} = \frac{A_{02}N_2}{A_{01}N_1}.\tag{1}$$

Here, N_1 and N_2 are the populations of levels |1> and |2>. A_{01} and A_{02} are the total spontaneous emission rate constants from levels |1> and |2> to level |0>. The populations N_1 and N_2 , are related by

^{*} Corresponding author.

^{**} Corresponding author. Department of Materials Science & Engineering, University of Washington, Seattle, WA, 98195, USA. E-mail address: peterpz@uw.edu (X. Xia).

¹ Department of Chemistry, Northwestern University, Evanston, IL, 60208, USA (present address).

$$\frac{N_2}{N_1} = \frac{g_2}{g_1} exp\left(-\frac{\delta E}{k_B T}\right),\tag{2}$$

where \mathcal{E}_1 and \mathcal{E}_2 are the degeneracies of the two levels and δE is the energy gap between the barycenters of the $|1>\rightarrow|0>$ and $|2>\rightarrow|0>$ emission bands. Consequently, the population in N_2 is small if $\delta E\gg kT$. Typically, the two excited states are considered to be thermally coupled (i.e., in a thermodynamic quasi-equilibrium state) for δE ranging from 200 to 2000 cm⁻¹ [9]. The temperature can be expressed as

$$\frac{1}{T} = -\frac{k_B}{\delta F} (ln\Delta - lnB), \tag{3}$$

where B is $\frac{A_{01}g_1}{A_{02}g_2}$. Both the B and δE parameters can be extracted following temperature calibrations.

The most common upconversion (UC) systems for LIR thermometry are based on Yb^{3+} as a sensitizer and Er^{3+} as an activator. Yb^{3+} acts as an effective sensitizer with a large absorption cross-section at 980 nm, a wavelength easily available due to its use in telecommunications industry for pumping erbium-doped fiber amplifiers. This wavelength also is widely used in biological systems because it lies in the tissue penetration window [4]. Furthermore, the Yb^{3+} excited state energy level matches well with the excited states of Er^{3+} ions, allowing a sequence of near-resonant energy transfers and the resulting stepwise excitation of Er^{3+} (Fig. 1). As an activator, Er^{3+} is one of the widely used ions due to its highly temperature-dependent and intense green emission arising from the thermally coupled ${}^2H_{11/2}$ and ${}^4S_{3/2}$ states, whose separation is about 800 cm $^{-1}$ [10]. The combination of Yb^{3+}/Er^{3+} is extensively

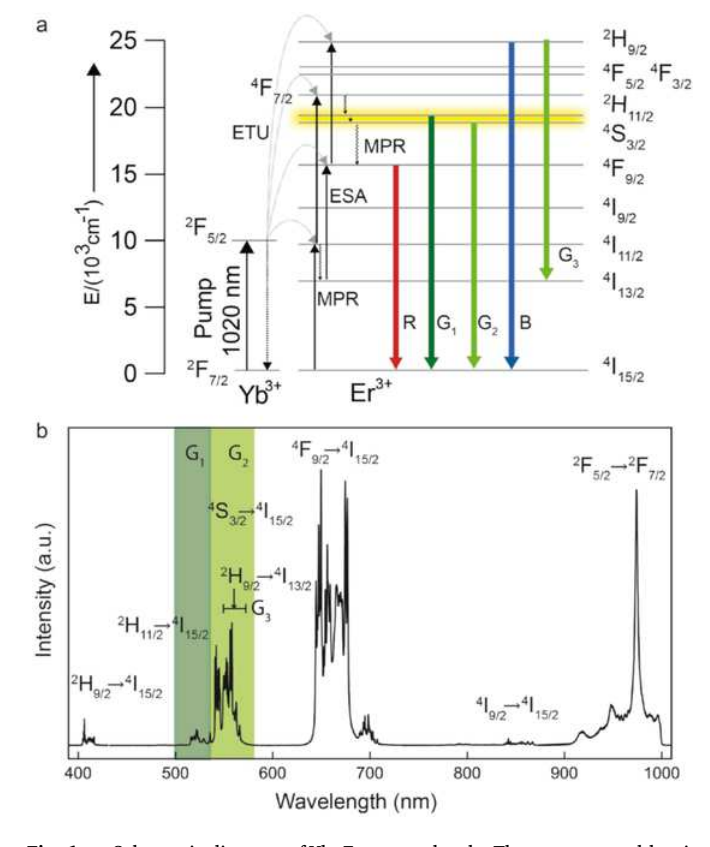


Fig. 1. a. Schematic diagram of Yb–Er energy levels. The upconverted luminescence involves green emissions from the thermally coupled $^2H_{11/2}$ and $^4S_{3/2}$ states for LIR thermometry (G1 and G2, respectively), red emission (R) from the $^4F_{9/2}$ state, and blue emission (B) from the $^2H_{9/2}$ state. The alternative relaxation of $^2H_{9/2}$ to the intermediate state $^4I_{13/2}$ also emits green light G_3 , overlapping with G_1 and G_2 . b. Representative PL spectrum of a $K_2LuF_5{:}10\%\,Yb,0.5\,\%Er$ doped crystal. The two green emission bands G_1 and G_2 for LIR analysis are highlighted.

used in a variety of host materials for LIR thermometry and their sensitivities are compared in the following references [11-14].

The intensity ratio of the ${}^2H_{11/2} \rightarrow {}^4I_{15/2}$ emission (labelled G1 in Fig. 1b at $\lambda=510$ –530 nm) and ${}^4S_{3/2} \rightarrow {}^4I_{15/2}$ emission (labelled G2 in Fig. 1b at $\lambda=535$ –570 nm) is utilized to determine the temperature of UC crystals. In addition to the green transitions, there are red, blue, and sometimes ultra-violet transitions as well, depending on lanthanide concentrations and also the lattice structures of the host materials. The blue and UV emissions, which require high UC efficiencies, are usually weaker than the green or red emission. For some UC crystals, the intensity ratio of the red and green emission bands is also used for optical thermometry [15].

The ${}^2H_{9/2}$ state, which emits blue light if it relaxes to the ground state, can also emit green light if it branches to the intermediate ${}^4I_{13/2}$ excited state. Such green emission from the ${}^2H_{9/2} \rightarrow {}^4I_{13/2}$ transition will interfere with the ratiometric thermometry bands and cause an inaccurate temperature readout. However, this has not been discussed extensively in the literature [16,17]. Renero et al. did spectroscopic characterizations of this emission in the hexa gonal phase Na YF₄ but quantifying the impact of this ${}^2H_{9/2} \rightarrow {}^4I_{13/2}$ emission in the context of optical thermometry has been limited [18]. In this work, we have characterized the impact of ${\rm Er}^{3+}\,{}^2H_{9/2} \rightarrow {}^4I_{13/2}$ emission on all-optical thermometry, including the interplay between upconversion pathways involving ${\rm Er}^{3+}\,{}^4F_{9/2},\,{}^2H_{11/2},\,{}^4S_{3/2}$ and ${}^2H_{9/2}$ states.

2. Experimental

Materials: $K_2LuF_5:x\%Yb$, 0.5%Er (x = 0–99) microcrystals were synthesized as described previously [19]. Briefly, lutetium nitrate hexahydrate (Lu(NO3·6H2O)3) and ytterbium nitrate hexahydrate (Yb(NO₃)₃·6H₂O) were of 99.99% purity and purchased from Sigma-Aldrich. Potassium hydroxide (KOH), potassium fluoride (KF), ethanol and oleic acid were analytical grade purchased from Sigma-Aldrich and used without further purification. 18.2 MΩ·cm Milli-Q deionized water was used for each synthesis. For a typical synthesis, 420.8 mg of KOH was dissolved in 1.5 mL of water, followed by 5 mL of ethanol and 5 mL of oleic acid with stirring. Then, 1.6 mL of 0.5 M RE(NO₃)₃ were added into the mixture. After stirring for 10 min, 1.89 g kF was dissolved in 3 mL water and added to the mixture dropwise. After additional agitation for 10 min, the resulting mixture was transferred to a 23 mL Teflon-lined autoclave and heated at 220°C for 24 h. After the autoclave cooled to room temperature, crystals were isolated by washing and centrifuging by ethanol and water three times. After drying the product at 60°C for 12 h, they were transferred to a Lindberg Blue tube furnace and heated at 300°C in air for 2 h to remove any residual organic surface ligands. The purity of the obtained compounds was confirmed by XRD.

Spectroscopic Measurements: NIR upconversion excitation at 1020 nm was provided by fiber coupled single mode laser diodes (QPhotonics, QFBGLD-1020-400). Direct excitation of $^4\mathrm{S}_{3/2}$ state at 532 nm was provided by a single longitudinal mode laser (Coherent Compass 532). Direct excitation of $^2\mathrm{H}_{9/2}$ state at 375 nm was provided by a Xe-lamp coupled to an Acton SpectraPro 300i monochromator. Emission spectra were acquired with an Acton SpectraPro 500i spectrograph with a Princeton liquid-nitrogen-cooled Si detector. Various excitation lasers were focused to a diffraction-limited spot (radius = 1.2 μm) using a long working distance 50X objective (Mitutoyo, M Plan Apo). Photoluminescence was collected by the same objective. Six spectra, collected for 0.5 ms each, were averaged to obtain the final PL spectrum.

Absorption spectra were collected using an Agilent Cary 5000 UV–Vis–NIR spectrometer with the sample powder loaded into a helium flow cryostat and cooled to around 80 K.

Time-resolved emission was generated with pulsed $1020~\mathrm{nm}$ excitation. A Tektronics function generator was used to control the laser

diode and generate laser pulses of 0.1 ms duration with a frequency of 10 Hz. An avalanche photodiode detector (Thorlabs APD430A) was used to collect the luminescence decay signal.

3. Results and discussion

3.1. ${}^{2}H_{9/2} \rightarrow {}^{4}I_{13/2}$ transition

The UC material used in this work is Yb/Er co-doped K₂LuF₅. Fig. 2 shows the photoluminescence (PL) spectra of a K₂LuF₅:10%Yb, 0.5%Er crystal and absorption of K₂ErF₅. The blue emission (400-420 nm) in Fig. 2a confirms a population of excited ²H_{9/2} states created following NIR excitation. It can relax to the 4I_{15/2} ground state and 4I_{13/2} intermediate excited state, emitting blue and green light respectively. However, such green emission is difficult to characterize because it overlaps with the ${}^2H_{11/2} \rightarrow {}^4I_{15/2}$ and ${}^4S_{3/2} \rightarrow {}^4I_{15/2}$ emissions of Er³⁺. To uniquely assign the additional green emission from ${}^{2}H_{9/2} \rightarrow {}^{4}I_{13/2}$ transition in this upconversion process, PL of the same sample excited by 375 nm and 532 nm laser were provided in Fig. 2 as well. Fig. 2a shows that the ²H_{9/2} state can be populated upon direct excitation with 375 nm light, whose photon energy is slightly higher than ${}^{2}H_{9/2}$. It can also be populated through NIR upconversion with 1020 nm excitation. However, there is no emission observed with 532 nm excitation because the excitation energy is either too low for the direct excitation, or too high to accomplish multi-photon upconversion. Although the 532 nm laser is not sufficient to excite the ²H_{9/2} directly, it can excite the ²H_{11/2} and ⁴S_{3/2} states, whose energy levels are lower than ²H_{9/2}. Therefore, the green emission upon 532 nm excitation is solely from the $^2H_{11/2} \rightarrow ^4I_{15/2}$ and $^4S_{3/2} \rightarrow ^4I_{15/2}$ transitions without any potential overlap with the ${}^2H_{9/2} \rightarrow {}^4I_{13/2}$ emission (Fig. 2b). In contrast, for both 375 nm and 1020 nm excitation wavelengths there are additional peaks compared to the PL with 532 nm excitation, highlighted by the vertical dashed lines in Fig. 2b. Since the two excitations can populate the ${}^{2}H_{9/2}$ state, these additional peaks must be related to ${}^{2}H_{9/2} \rightarrow {}^{4}I_{13/2}$

Crucially, the absence of corresponding absorption peaks in Fig. 2c (red arrows) confirms the nature of this emission from a higher excited state to an intermediate excited state, instead of relaxing to the ground state. At room temperature all of the $\rm Er^{3+}$ ions are in the $^4\rm I_{15/2}$ ground state. There is no absorption from the intermediate excited state to a higher excited state. This demonstrates why the emission from the $^2\rm H_{9/2} \rightarrow ^4\rm I_{13/2}$ transition lacks the corresponding absorption in the same wavelength range while emission and absorption peaks are well matched for the $^2\rm H_{11/2} \rightarrow ^4\rm I_{15/2}$ and $^4\rm S_{3/2} \rightarrow ^4\rm I_{15/2}$ transitions.

The relative intensity of these peaks compared to the ${}^2H_{11/2} \rightarrow {}^4I_{15/2}$ and ${}^4S_{3/2} \rightarrow {}^4I_{15/2}$ increases with the ytterbium doping concentration. The ${}^2H_{9/2} \rightarrow {}^4I_{13/2}$ emission stands out at high Yb³⁺ concentrations, which helps identify all possible ${}^2H_{9/2} \rightarrow {}^4I_{13/2}$ peaks. In Fig. 3a, thir-

teen peaks have been assigned to the ${}^2H_{9/2} \rightarrow {}^4I_{13/2}$ transition by comparing the emission with different Yb³+ concentrations. Besides these peaks, a total of 26 peaks in the green spectral region between 530 nm and 570 nm are identified and Lorentzian fitted to obtain the center wavelengths and FWHM parameters of the ${}^2H_{9/2} \rightarrow {}^4I_{13/2}$ emission for further subtraction from the raw overlapping PL spectrum. Fig. 3b shows the sum of 13 fitted Lorentzian peaks (green) from ${}^2H_{9/2} \rightarrow {}^4I_{13/2}$ emission. Residual emission (red) following the subtraction of ${}^2H_{9/2} \rightarrow {}^4I_{13/2}$ peaks is identical to the PL with 532 nm excitation (Fig. 2b) and the PL from samples without Yb dopant ions (Fig. 3a), indicating emission solely from the ${}^4S_{3/2} \rightarrow {}^4I_{15/2}$ transition.

3.2. Power- and temperature-dependence

Emission from the ${}^{2}H_{9/2} \rightarrow {}^{4}I_{13/2}$ transition has a different power dependence from the ${}^2H_{11/2} \rightarrow {}^4I_{15/2}$ and ${}^4S_{3/2} \rightarrow {}^4I_{15/2}$ transitions that are widely used in LIR thermometry. Fig. 4a plots Er³⁺ PL at various excitation powers. All spectra are normalized by the maximum intensity of the ${}^{2}H_{11/2} \rightarrow {}^{4}I_{15/2}$ (G₁) emission at 523 nm. The emission between 539 nm and 549 nm is assigned only to the ${}^4S_{3/2} \rightarrow {}^4I_{15/2}$ transition labelled $G_2(1),$ not effected by the $^2H_{9/2} \rightarrow \,^4I_{13/2}$ emission. The spectral range between 550 nm and 570 nm arises from overlapping $^4\mathrm{S}_{3/2} \rightarrow ^4\mathrm{I}_{15/2}$ and $^2\mathrm{H}_{9/2} \rightarrow ^4\mathrm{I}_{13/2}$ transitions labelled $\mathrm{G}_2(2) + \mathrm{G}_3$. The emission intensities for both the G₁ and G₂(1) regions have the same power dependence while the mixed $G_2(2) + G_3$ emission intensity increases much more rapidly. Temperature-dependent Er³⁺ PL in Fig. 4b confirms such different intensity responses of $G_2(1)$ and $G_2(2) + G_3$ to excitation powers in Fig. 4a are not caused by radiation-induced internal temperature changes, because the relative intensity of both G₂(1) and $G_2(2) + G_3$ have the same response to temperature. Consequently, the observed power dependence of the overlapping ${}^{2}H_{9/2} \rightarrow {}^{4}I_{13/2}$ emission will cause significant complications for non-contact optical thermometry using Er³⁺ ions, discussed in more detail below.

To evaluate the impact of ${}^2H_{9/2} \rightarrow {}^4I_{13/2}$ emission on erbium-based LIR thermometry, KLF samples were sealed in a cryostat to measure their LIR response as a function of temperature. Fig. 5a illustrates the experimental setup. During the temperature calibration measurement, the laser irradiance was kept constant to a low value (3 kW/cm²) in order to minimize any photothermal effects from the laser. Logarithms of PL intensity ratios as a function of the reciprocal of temperature are given in Fig. 5b, where the linear fittings are used to interpret the temperatures of the same sample with increasing excitation irradiance in Fig. 5c. Two ratios with different sets of wavelength intervals are used in the temperature calibration, namely G_1/G_2 and $G_1/(G_2+G_3)$, where G refers to the integrated green PL over the specified range. The ${}^2H_{11/2} \rightarrow {}^4I_{15/2}$ interval is 515 nm–530 nm (G_1) for both analyses, while two different intervals of ${}^4S_{3/2} \rightarrow {}^4I_{15/2}$ emission are used. In the first analysis, the exclusive ${}^4S_{3/2} \rightarrow {}^4I_{15/2}$ emission between 540 nm and

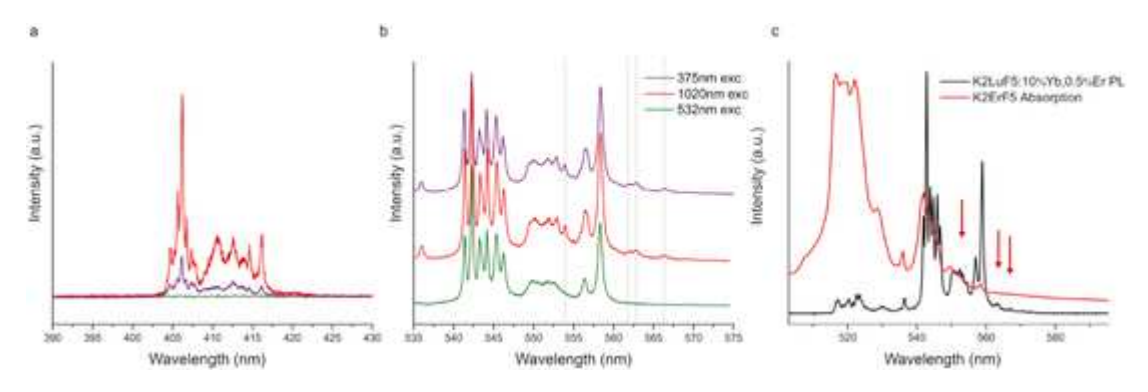


Fig. 2. PL spectra of a K_2LuF_5 :10% Yb, 0.5% Er crystal with 1020 nm (red), 375 nm (purple), and 532 nm (green) excitations at a) 400 nm -420 nm ($^2H_{9/2} \rightarrow ^4I_{15/2}$) and b) 535 nm -570 nm ($^2H_{9/2} \rightarrow ^4I_{13/2}$) wavelength ranges. c) PL from a K_2LuF_5 :10% Yb, 0.5% Er crystal with an excitation laser of 1020 nm (black) and absorption of a K_2ErF_5 pellet (red). PL in 560 nm -570 nm range (highlighted by red arrows) lacks corresponding absorption peaks, suggesting the emission from a higher excited state to an intermediate excited state.

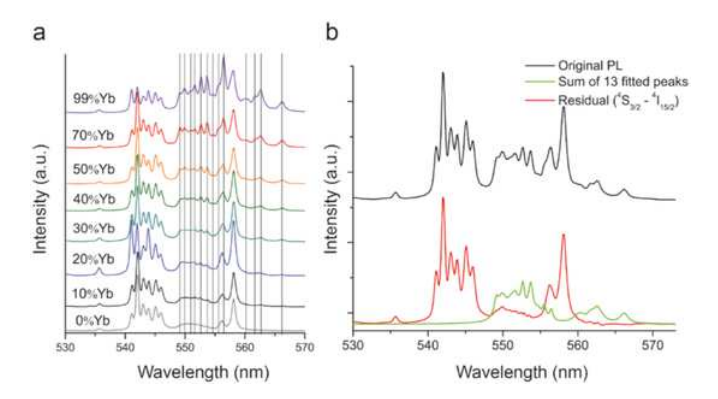


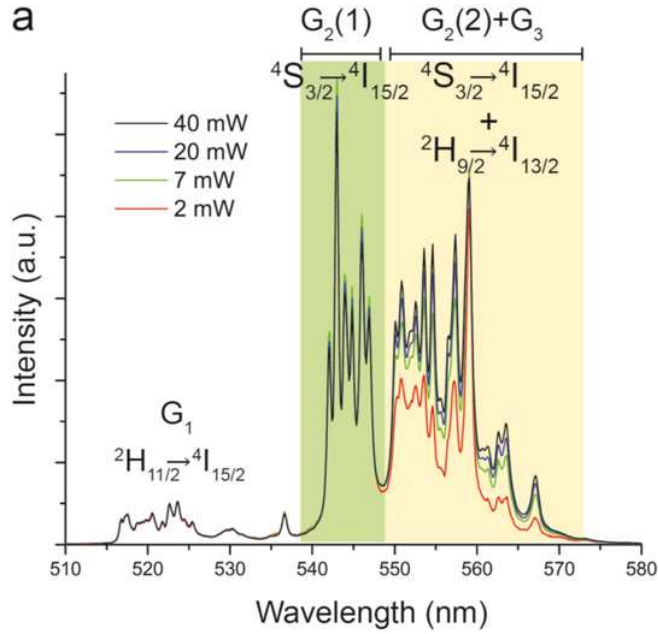
Fig. 3. a) Er PL with increased Yb^{3+} concentration. Additional peaks arise in 550 nm–570 nm range with higher Yb dopant concentration. All PL were collected with a very low irradiance. b) Fitting and subtraction of the additional peaks in a) After subtraction, the PL is the same as 0% Yb, 0.5% Er doped sample.

549 nm is used. The second analysis 540–570 nm is used to cover the full $^4S_{3/2} \rightarrow ^4I_{15/2}$ emission, which overlaps with the $^2H_{9/2} \rightarrow ^4I_{13/2}$ emission G_3 .

The two calibration methods based on different wavelength intervals have similar slopes. However, their LIR responses are observed to differ significantly as a function of laser irradiance. In Fig. 5c, the temperature interpreted from the G_1/G_2 ratio indicates heating when the KLF crystal is pumped with increasing laser irradiance. However, if the LIR analysis includes emission from the overlapping ${}^{2}\text{H}_{9/2} \rightarrow {}^{4}\text{I}_{13/2}$ transition, namely $G_1/(G_2+G_3)$, then an opposite cooling trend is observed, which contradicts with the result without ${}^{2}H_{9/2} \rightarrow {}^{4}I_{13/2}$ overlap. Increasing excitation power is used here because the internal temperature change, no matter heating or cooling, is positively correlated to power density [20]. At the low irradiances (<0.1 MW cm⁻²) of 1020 nm laser, the spectral overlap has a negligible effect. However, at the higher laser irradiances used for laser cooling, the effect becomes important (Fig. 5c) despite the lower absorption coefficient of Yb(III) ions at the laser cooling excitation wavelength of 1020 nm. Typically, irradiance of 1–100 W·cm⁻²([1,6]) is used for luminescence thermometry at the excitation wavelength of 980 nm. Such spectral overlap may be negligible considering the low irradiances. However, the absorption coefficient of Yb(III) ions at 980 nm is much higher than 1020 nm used in this work, which may result in non-negligible spectral overlap even at low irradiances.

Similar measurements were performed on crystals with various Yb^{3+} concentrations in order to further evaluate the impact of ${}^2H_{9/2}$ upconversion on LIR thermometry. A decrease in the $G_1/(G_2+G_3)$ ratio was observed in samples as Yb^{3+} concentrations were increased from 10% to 99% (Fig. 5d). A simple consideration of this decrease in the $G_1/(G_2+G_3)$ ratio would indicate that solid state laser cooing is possible at Yb doping levels of 99%. However, to the best of our knowledge the laser refrigeration of crystals with Yb^{3+} concentration higher than 10% has never been reported in the literature [21,22] due to non-radiative relaxation that stems from concentration quenching. The measured lifetime of Yb^{3+} also decreases with increased Yb^{3+} concentration, consistent with prior reports of concentration quenching at elevated Yb^{3+} concentrations [21]. These lifetime data contradict the simple interpretation of laser cooling based on the $G_1/(G_2+G_3)$ ratio.

The observations above highlight the crucial importance of using the $^4S_{3/2} \rightarrow ^4I_{15/2}$ emission without overlapping $^2H_{9/2} \rightarrow ^4I_{13/2}$ emission in LIR thermometry based on Er $^{3+}$ ions. The major impact that the $^2H_{9/2} \rightarrow ^4I_{13/2}$ transition has on Er $^{3+}$ based optical thermometry arises from the different upconversion mechanism of $^2H_{9/2}$ from $^2H_{11/2}$ and $^4S_{3/2}$ states. During the energy transfer up-conversion (ETU), one excited Yb $^{3+}$ ion relaxes to its ground state while simultaneously exciting an Er $^{3+}$ ion. This ETU process can occur several times in succession, re-



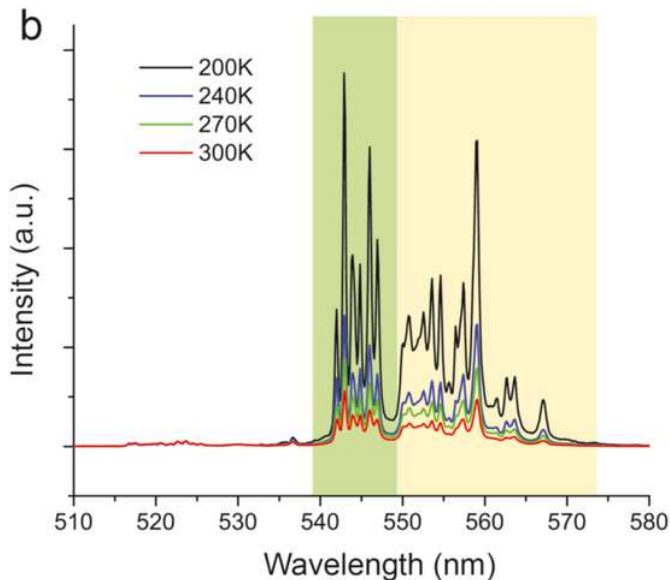


Fig. 4. a) Er³⁺ PL excited by various laser powers. All spectra in a) and b) are normalized by the intensity of ${}^2H_{11/2} \rightarrow {}^4I_{15/2}$ emission (G_1). With high excitation powers, the normalized intensity of the first half of ${}^4S_{3/2} \rightarrow {}^4I_{15/2}$ emission ($G_2(1)$) remains the same, while the second half of ${}^4S_{3/2} \rightarrow {}^4I_{15/2}$ emission ($G_2(2)$) and ${}^2H_{9/2} \rightarrow {}^4I_{13/2}$ emission (G_3) increase. b) Er³⁺ PL at different temperatures. The excitation power is kept at 2 mW. The relative intensity $G_2(1)$, $G_2(2)$ and G_3 to the G_1 share similar response to temperature.

sulting in an Er^{3+} ion excited to the ${}^{2}H_{9/2}$ state, which is reached after at least three energy transfer steps with a similar excitation wavelength [23].

The number of energy transfer steps, or photons required in the upconversion process, can be studied by measuring the emission intensity at various powers. Although it is difficult to characterize the ${}^2{\rm H}_{9/2} \rightarrow {}^4{\rm I}_{13/2}$ transition due to overlap with other emissions, the blue emission around 410 nm from the same ${}^2{\rm H}_{9/2}$ excited state can be measured to study its upconversion mechanisms. The slopes of the double logarithmic plots of red, green, and blue emission in Fig. 6b suggest that the ${}^2{\rm H}_{9/2}$ upconversion is a 3- or 4-photon process, while the ${}^2{\rm H}_{11/2}$ and ${}^4{\rm S}_{3/2}$ upconversions are 2- or 3-photon process. Although it is challenging to quantify the exact number of photons in these upconversion

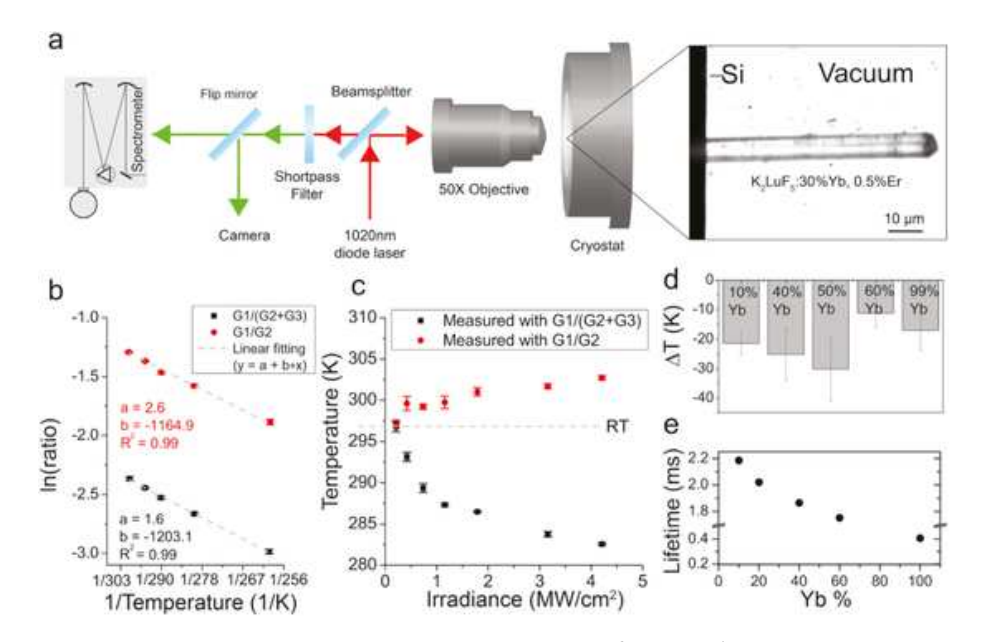


Fig. 5. a) PL measurement setup. b) Temperature calibrations using ratios of the ${}^2H_{11/2} \to {}^4I_{15/2}$ emission intensity to the total intensity of ${}^4S_{3/2} \to {}^4I_{15/2}$ full emission overlapping with ${}^2H_{9/2} \to {}^4I_{13/2}$ emission (ln[$G_1/(G_2+G_3)$], black), and to the first half of ${}^4S_{3/2} \to {}^4I_{15/2}$ emission without additional ${}^2H_{9/2} \to {}^4I_{13/2}$ emission overlap (ln[$G_1/(G_2)$], red). c) Calibrated temperatures of the crystal excited by increased 1020 nm laser power with two different Er³⁺ PL ranges. The selection of wavelength intervals results in opposite temperature interpretations. d. The misinterpreted temperatures of K_2LuF_5 :0.5%Er/x%Yb crystals doped with various Yb concentrations using intensity ratios of $G_1/(G_2+G_3)$. e. Decreasing lifetime of the Yb³⁺ ${}^2F_5/2$ state of K_2LuF_5 :crystals with increasing Yb% due to concentration quenching.

processes, the slope of blue emission is always higher than that of the green and red emissions. The different amounts of photons required agrees with power-dependent measurements performed with 1.54 μ m excitation showing that ground state luminescence from $^2H_{9/2}$ and $^4S_{3/2}$ involve 4-photon and 3-photon upconversion, respectively [24].

There are different possible upconversion pathways to the ${}^2H_{9/2}$ state [25]. The most accepted one proposes that the ${}^4F_{9/2}$ level is the initial state in the energy transfer step leading to the ${}^2H_{9/2}$ state [26–28]. Therefore, upconversion to ${}^2H_{9/2}$ requires at least one more photon than to the ${}^4F_{9/2}$, ${}^2H_{11/2}$, and ${}^4S_{3/2}$ levels. This explains the larger slope of ${}^2H_{9/2} \rightarrow {}^4I_{13/2}$ emission in the 550 nm–570 nm spectral region in comparison with the ${}^2H_{11/2} \rightarrow {}^4I_{15/2}$ and ${}^4S_{3/2} \rightarrow {}^4I_{15/2}$ transitions with increasing excitation power. If the ${}^2H_{9/2} \rightarrow {}^4I_{13/2}$ emission is included in the LIR analysis, it will lead to an incorrect interpretation of the temperature. The same problem arises for Er³⁺ thermometry using red/green emission ratios [15].

3.3. Implications for Yb/Er LIR thermometry

In recent years more advanced LIR techniques have been reported based on temperature-dependent luminescence intensity distributions, such as differential luminescence thermometry that monitors time-differencing luminescence [29]. However, the wavelength overlap of $^4\mathrm{S}_{3/2} \to ^4\mathrm{I}_{15/2}$ and $^2\mathrm{H}_{9/2} \to ^4\mathrm{I}_{13/2}$ emission cannot be avoided. Careful wavelength interval selection or $^2\mathrm{H}_{9/2} \to ^4\mathrm{I}_{13/2}$ emission subtraction must be done for accurate temperature measurement. Perhaps the best solution is to fix the pump power and avoid a power dependent temperature measurement. However, for some applications, such as examining the cooling properties of micro- or nano-size laser cooling materials, a power dependent measurement cannot be avoided. A pump-probe method in a confocal system [4] can be applied that an additional constant power probe laser is used and only the PL excited by the probe laser is collected via the confocal setup.

The host materials and dopant concentrations must also be considered. Overlap of ${}^2H_{9/2} \rightarrow {}^4I_{13/2}$ and ${}^4S_{3/2} \rightarrow {}^4I_{15/2}$ emissions is also observed in other popular fluoride host materials such as NaYF4 [4,17] and LiYF₄, and in oxide host materials [16]. Recent work suggests that

the lattice phonon energy strongly affects the red emission intensity and also the energy transfer efficiency to the ${}^4F_{9/2}$ [28,30], which is the intermediate excited state before upconverting to the ${}^2H_{9/2}$ state. Host materials with low lattice phonon energies are preferred. The sensitizer Yb $^{3+}$ concentration should be lower than 20% to avoid energy clustering, i.e., excitation energy is preserved in a sub-lattice domain of Yb $^{3+}$ clusters, which enhances upconversion to ${}^2H_{9/2}$ [31].

4. Conclusion

We have demonstrated the existence of $^2H_{9/2} \rightarrow ^4I_{13/2}$ green PL in Yb $^{3+}/Er^{3+}$ co-doped K $_2LuF_5$. At room temperature, this emission covers a wide wavelength range (545 nm–570 nm) such that it overlaps the $^4S_{3/2} \rightarrow ^4I_{15/2}$ emission. Peaks at 560 nm–570 nm do not overlap with other transitions and are characteristics of $^2H_{9/2} \rightarrow ^4I_{13/2}$ emission. Such emission exists not only in K_2LuF_5 microcrystals but also other Yb $^{3+}/Er^{3+}$ co-doped fluoride and oxide materials.

We have shown that ${}^2H_{9/2} \rightarrow {}^4I_{13/2}$ emission is more sensitive to pump power than ${}^2H_{11/2} \rightarrow {}^4I_{15/2}$ and ${}^4S_{3/2} \rightarrow {}^4I_{15/2}$ emission because it requires more energy-transfer steps during upconversion. It leads to incorrect temperature readout when this emission is included in the LIR analysis, especially when high pump powers are used.

Finally we conclude that the LIR wavelength intervals need to be examined carefully to avoid the overlapping emission from ${}^2H_{9/2} \rightarrow {}^4I_{13/2}$. Suggestions have been made on optical experimental setup and selection of host materials and dopant concentrations.

Author statement

Xiaojing Xia: Conceptualization, Investigation, Data curation, Methodology, Visualization, Writing – original draft, Software, Azzurra Volpi: Supervision, Methodology, Joo Yeon D. Roh: Data curation. Michael De Siena: Data curation. Daniel R. Gamelin: Reviewing and Editing, Resources, Supervision, Funding acquisition, Markus P. Hehlen: Reviewing and Editing, Resources, Supervision, Peter J. Pauzasukie: Conceptualization, Supervision, Writing – review & editing, Resources, Funding acquisition.

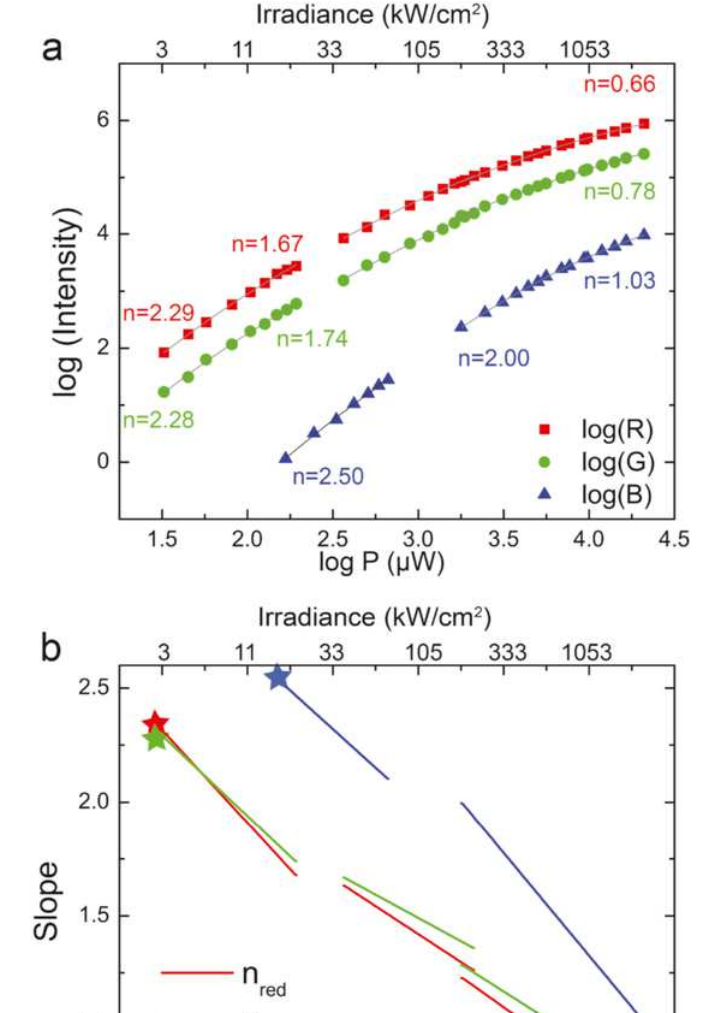


Fig. 6. a) Double logarithmic plots of red, green, and blue emission intensities versus 1020 nm laser power. b). The slopes of the double logarithmic plots. The higher slope of the blue emission compared to the green emission suggests the different power response of $^2H_{9/2} \rightarrow ^4I_{13/2}$ from other $^2H_{11/2} \rightarrow ^4I_{15/2}$ and $^4S_{3/2} \rightarrow ^4I_{15/2}$ green emissions. The population of the $^2H_{9/2}$ excited state involves 3- or 4-photon upconversion.

2.5

3.0

log P (µW)

3.5

4.0

4.5

Declaration of competing interest

n_{blue}

2.0

The authors declare that they have no known competing financial interests or personal relationships that could have appeared to influence the work reported in this paper.

Acknowledgements

1.0

1.5

X.X., P.J.P., A.V., and M.P.H. acknowledge support from the MURI:MARBLe project under the auspices of the Air Force Office of Scientific Research (Award #FA9550-16-1-0362). This research was partially supported by the National Science Foundation (NSF) through the UW Molecular Engineering Materials Center, a Materials Research Science and Engineering Center (DMR-1719797, to D.R.G. and P.J.P.). X.X. and P.J.P. acknowledge support from the UW Nano-engineered systems institute. Part of this work was conducted at the Molecular

Analysis Facility, a National Nanotechnology Coordinated Infrastructure site at the University of Washington which is supported in part by the National Science Foundation (grant NNCI-1542101), the University of Washington, the Molecular Engineering Sciences Institute, and the Clean Energy Institute.

References

- [1] C. D. Brites, S. Balabhadra, L. D. Carlos, Lanthanide-Based Thermometers: at the Cutting-Edge of Luminescence Thermometry, 2019, https://doi.org/10. 1002/adom.201801239.
- [2] S. Baral, S.C. Johnson, A.A. Alaulamie, H.H. Richardson, Nanothermometry using optically trapped erbium oxide nanoparticle, Appl. Phys. A 122 (2016) 340.
- [3] E.J. McLaurin, L.R. Bradshaw, D.R. Gamelin, Dual-emitting nanoscale temperature sensors, Chem. Mater. 25 (2013) 1283–1292.
- [4] F. Vetrone, R. Naccache, A. Zamarrón, A. Juarranz de la Fuente, F. Sanz-Rodríguez, L. Martinez Maestro, E. Martin Rodriguez, D. Jaque, J. Garcia Sole, J.A. Capobianco, Temperature sensing using fluorescent nanothermometers, ACS Nano 4 (2010) 3254–3258.
- [5] S. Collins, G. Baxter, S. Wade, T. Sun, K. Grattan, Z. Zhang, A. Palmer, Comparison of fluorescence-based temperature sensor schemes: theoretical analysis and experimental validation, J. Appl. Phys. 84 (1998) 4649–4654.
- [6] J. Zhou, B. Del Rosal, D. Jaque, S. Uchiyama, D. Jin, Advances and challenges for fluorescence nanothermometry, Nat. Methods (2020) 1–14.
- [7] M. Jia, G. Liu, Z. Sun, Z. Fu, W. Xu, Investigation on two forms of temperature-sensing parameters for fluorescence intensity ratio thermometry based on thermal coupled theory, Inorg. Chem. 57 (2018) 1213–1219.
- [8] S.A. Wade, S.F. Collins, G.W. Baxter, Fluorescence intensity ratio technique for optical fiber point temperature sensing, J. Appl. Phys. 94 (2003) 4743–4756.
- [9] A. Khalid, K. Kontis, 2d surface thermal imaging using rise-time analysis from laser-induced luminescence phosphor thermometry, Meas. Sci. Technol. 20 (2009) 025305.
- [10] H. Berthou, C. Jörgensen, Optical-fiber temperature sensor based on upconversion-excited fluorescence, Optic Lett. 15 (1990) 1100–1102.
- [11] A. Siaï, P. Haro-González, K.H. Naifer, M. Férid, Optical temperature sensing of ${\rm Er^{3+/Yb^{3+}}}$ doped LaGdO $_3$ based on fluorescence intensity ratio and lifetime thermometry, Opt. Mater. 76 (2018) 34–41.
- [12] Y. Ma, G. Xiang, J. Zhang, Z. Liu, P. Zhou, W. Liu, X. Tang, S. Jiang, X. Zhou, L. Li, et al., Upconversion properties and temperature sensing behaviors in visible and near-infrared region based on fluorescence intensity ratio in LuVO 4:Yb³⁺/Er³⁺, J. Alloys Compd. 769 (2018) 325–331.
- [13] M. Quintanilla, E. Cantelar, F. Cusso, M. Villegas, A.C. Caballero, Temperature sensing with up-converting submicron-sized LiNbO₃: Er³⁺/Yb³⁺ particles, APEX 4 (2011) 022601.
- [14] P. Dos Santos, M. De Araujo, A. Gouveia-Neto, J. Medeiros Neto, A. Sombra, Optical temperature sensing using upconversion fluorescence emission in Er³⁺/Yb³⁺-codoped chalcogenide glass, Appl. Phys. Lett. 73 (1998) 578–580.
- [15] A. C. Brandão-Silva, M. A. Gomes, S. M. Novais, Z. S. Macedo, J. F. Avila, J. Rodrigues Jr., M. Alencar, Size influence on temperature sensing of erbium-doped yttrium oxide nanocrystals exploiting thermally coupled and uncoupled levels' pairs, J. Alloys Compd. 731 (2018) 478–488.
- [16] X. Mateos, R. Solé, J. Gavaldà, M. Aguiló, F. Díaz, J. Massons, Ultraviolet and visible emissions of Er³⁺ in KY (WO₄)₂ single crystals co-doped with Yb³⁺ ions, J. Lumin. 115 (2005) 131–137.
- [17] S. Zhou, K. Deng, X. Wei, G. Jiang, C. Duan, Y. Chen, M. Yin, Upconversion luminescence of NaYF₄:Yb³⁺, Er³⁺ for temperature sensing, Optic Commun. 291 (2013) 138–142.
- [18] C. Renero-Lecuna, R. Martín-Rodríguez, R. Valiente, J. González, F. Rodríguez, K. Kramer, H. Gudel, Origin of the high upconversion green luminescence efficiency in β-NaYF₄: 2% Er³⁺, 20% Yb³⁺, Chem. Mater. 23 (2011) 3442–3448.
- [19] X. Xia, A. Pant, X. Zhou, E. Dobretsova, A. Bard, M. Lim, J.Y. Roh, D.R. Gamelin, P. Pauzauskie, Hydrothermal Synthesis and Solid-State Laser Refrigeration of Ytterbium-Doped Potassium Lutetium Fluoride (KLF) Microcrystals, 2020 ChemRxiv.
- [20] Y. Cui, L. Zheng, W. Xu, H. Liu, L. Li, Z. Zhang, Influence of 980 nm pump power on optical thermometry based on NaYF₄:Yb³⁺/Er³⁺ nanoparticles, Mater. Res. Express 5 (2018) 065018.
- [21] D.V. Seletskiy, R. Epstein, M. Sheik-Bahae, Laser cooling in solids: advances and prospects, Rep. Prog. Phys. 79 (2016) 096401.
- [22] X. Xia, A. Pant, A.S. Ganas, F. Jelezko, P.J. Pauzauskie, Quantum point defects for solid-state laser refrigeration, Adv. Mater. (2020) 1905406.
- [23] J. Suyver, J. Grimm, K. Krämer, H.-U. Güdel, Highly efficient near-infrared to visible up-conversion process in NaYF₄:Er³⁺, Yb³⁺, J. Lumin. 114 (2005) 53–59.
- [24] M. Pollnau, D.R. Gamelin, S. Lüthi, H. Güdel, M.P. Hehlen, Power dependence of upconversion luminescence in lanthanide and transition-metalion systems, Phys. Rev. B 61 (2000) 3337.
- [25] M. T. Berry, P.S. May, Disputed mechanism for NIR-to-red upconversion luminescence in NaYF₄: Yb³⁺/Er³⁺, J. Phys. Chem. 119 (2015) 9805–9811.
- [26] V.M. Lojpur, P.S. Ahrenkiel, M.D. Dramićanin, Color-tunable up-conversion emission in Y₂O₃:Yb³⁺, Er³⁺ nanoparticles prepared by polymer complex

- solution method, Nanoscale Res. Lett. 8 (2013) 131.

 [27] M. Yuan, R. Wang, C. Zhang, Z. Yang, W. Cui, X. Yang, N. Xiao, H. Wang, X. Xu, Exploiting the silent upconversion emissions from a single β-NaYF₄: yb/Er microcrystal via saturated excitation, J. Mater. Chem. C 6 (2018) 10226–10232.
- [28] G. Liu, Advances in the theoretical understanding of photon upconversion in rare-earth activated nanophosphors, Chem. Soc. Rev. 44 (2015) 1635–1652.
 [29] W. Patterson, D. Seletskiy, M. Sheik-Bahae, R. Epstein, M. Hehlen, Measurement of solid-state optical refrigeration by two-band differential luminescence thermometry, JOSA B 27 (2010) 611–618.
- [30] H. Wu, Z. Hao, L. Zhang, X. Zhang, Y. Xiao, G.-H. Pan, H. Wu, Y. Luo, H. Zhao, J. Zhang, Phonon energy dependent energy transfer upconversion for the red emission in the $\rm Er^{3+}/Yb^{3+}$ system, J. Phys. Chem. C 122 (2018) 9611-9618.
- [31] J. Wang, R. Deng, M. A. MacDonald, B. Chen, J. Yuan, F. Wang, D. Chi, T.S. A. Hor, P. Zhang, G. Liu, et al., Enhancing multiphoton upconversion through energy clustering at sublattice level, Nat. Mater. 13 (2014) 157–162.